SEMARAK ILMU PUBLISHING

Journal of Advanced Research in Applied Sciences and Engineering Technology

Journal homepage:
https://semarakilmu.com.my/journals/index.php/applied_sciences_eng_tech/index
ISSN: 2462-1943

Influence of Compound Spherical Trenched Holes on Film Cooling Performance at the end of Combustor Simulator

Nor Azwadi Che sidik[1], Ehsan kianpour[2,*]

[1] Malaysia–Japan International Institute of Technology (MJIIT), Universiti Teknologi Malaysia, Jalan Sultan Yahya Petra, 54100 Kuala Lumpur, Malaysia
[2] Department of Mechanical Engineering, Najafabad Branch, Islamic Azad University, Najafabad, Iran

ABSTRACT

The major effects of cylindrical and spherical trenched cooling holes with distance between the hole surface and the combustion chamber panel and the filler diameter on the spherical hole contact surface and the panel surface H=0.3,R=D/2=0.1, H=0.3, R=D/2=0.2 and H=0.3, R=D/2=0.3 cm at BR=3.18 on the film cooling effectiveness near the combustor end wall surface is an important subject to study in details. In this research, a three-dimensional representation of a Pratt and Whitney gas turbine engine was simulated and analysed with a commercial finite volume package FLUENT 6.2.26. The analyses were done with RANS turbulence model on internal cooling passages. The combustor simulator was combined with the interaction of two rows of dilution jets, which were staggered in the streamwise direction and aligned in the spanwise direction. In comparison with the baseline case, the application of trenched holes increased the effectiveness of film cooling up to 47% near the wall surface and an average of 35% in depth of combustor simulator.

Keywords:
Gas Turbine Engine; Film-Cooling;
Trench Hole; Dilution Hole

Received: 2 June 2022 **Revised: 21 August 2022** **Accepted: 1 Sept 2022** **Published: 10 Sept 2022**

1. Introduction

Advanced gas turbine industries are trying hard for higher engine efficiencies. Brayton cycle is a key to achieve this purpose. In this cycle, to have higher gas turbine engine efficiency, the combustor ‘s outlet temperature must be increased [1]. But such hot flows cause non-uniformities at the end of the combustor and the inlet of the turbine and damage the critical parts. Film cooling is the most well-known method of preservation. In this technique, a low temperature thin layer attaches on a surface and protects it against hot streams. To get better film cooling performance, it is needed to increase blowing ratio. Blowing ratio increment has an intense effect on the heat transfer, particularly in the hole region. Due to the importance of this study, a broad literature survey was done to get the fundamental data related to film cooling performance. Harrington *et al*. [2] presented a simulated flat plate. The research was a computational and experimental one aimed at investigating a full

* *Corresponding author.*
E-mail address: ekianpour@gmail.com

https://doi.org/10.37934/araset.28.1.1324

coverage of adiabatic film cooling effectiveness. The focus of the findings was on the effects of ten rows of normal short cooling holes with a length of l/D = 1.0 at large density coolant jets and high mainstream turbulence intensity. The test results indicated that considering the blowing ratio, the maximum adiabatic film cooling effectiveness was attained near the area, which covered four to eight rows of cooling holes. Furthermore, the interaction of injected flows sprayed from the cooling rows limits the maximum effectiveness. On the other hand, film cooling effectiveness on the curved surface was investigated numerically by Koc *et al*. [3]. They highlighted that the curvature of the surface and the blowing ratio affect the film cooling effectiveness.

In another study, Azzi and Jurban [4] forecasted the film cooling thermal fields for a simulated cylindrical cooling row with the following ratios: extended range of length to diameter = 1.75/8, and fixed pitch to diameter = 3.0. The inclination angle was 35 degrees and the film hole was 12.7 mm in diameter. Another finding by Bernsdorf *et al*., [5] showed that in short cooling injection holes, effectiveness of film cooling is related to the injection hole length and angle. Tarchi *et al*. [6] investigated the effects of large dilution holes. These holes were placed within the injecting slot and eruption array. The flat plate cross section duct contained 270 cooling holes located in 29 staggered rows. The holes were 1.65 mm in diameter and had a length to diameter ratio of 5.5 and a stream-wise angle of 30 degrees. The dilution hole was 18.75 mm in diameter. It was located at the 14^{th} row of cooling holes. They showed that with using backward step, at downstream the dilution hole the adiabatic film cooling effectiveness reached to η_{aw}=0.65. Vakil and Thole [7] presented experimental results of the study of temperature distribution inside a combustor simulator.

In this study, a real large scale of combustor was modelled. This model contained four different cooling panels with many cooling holes. Two rows of dilution jets could be seen in the second and third cooling panels. The first row had three dilution jets and the second one had two jets. While the first and second panels were flat, two other panels angled with an angle of 15.8 degrees. In this study, a real large scale of combustor was simulated and high momentum dilution jets and the coolant flow were injected into the main flow. The results indicated that high temperature gradient was developed upstream of the dilution holes. Kianpour *et al*. [8,9] re-simulated the Vakil and Thole's combustor. They offered various geometries of cooling holes. The temperatures near the wall and among the jets were higher for the baseline cooling whereas the central part of the jets was cooler in trench cases. In a different study, Schuchkin *et al*. [10] investigated film cooling effectiveness in ultrasonic flow. The results showed that with Mach number increasing, shell friction coefficient, diffusion ratio, and turbulence intensity at the boundary film cooling decreased. Porosity reduces shell friction and mixing and thus improving the cooling effectiveness of the layer.

In 2018, Li *et al*. [11] numerically studied the film cooling effectiveness of a layer with shaped holes during the end cross-flows of the end wall. They found that despite the creation of negative vortices and jet vortices in the internal crossover flow resulting from the simulation of the flow in the turbine blade environment, the reuse of these end wall currents affects the film cooling effectiveness. Fraas *et al*. [12] experimentally studied the film cooling performance improvement by using an optimized cooling hole inlet geometry. The results showed that the cooling hole inlet geometry tremendously affects cooling performance. Diffuser aerodynamics are altered for all investigated geometries with a modified inlet. This leads to a more symmetrical pattern of the film cooling jet for two of the investigated geometries. Chen *et al*. [13] studied film cooling effectiveness distribution for a gas turbine blade under the effects of unsteady wakes and oncoming free-stream turbulence intensities using pressure sensitive paint (PSP) technique. Results showed that the effect of the mass flux ratio on the film cooling effectiveness decreases under the high turbulence intensity and unsteady wake conditions. Kim *et al*. [14] experimentally studied the effects of a protrusion installed at the slot exit on the film cooling effectiveness of inclined slots. Injection angles of 30° and

45° were considered for the slot, and a protrusion that induces the effects of free jet emerges close to a surface was installed at the slot exit. The film cooling effectiveness of the 45° inclined slot was improved by about 6.6% by installing a protrusion immediately after the slot exit.

2. Methodology

2.1 Model Description

In the present study, the combustor simulator applied was a 3-D representation of a Prat and Whitney gas turbine engine. In a real combustor, film cooling jets are used to form a low temperature layer of air that covers the combustor's inner and outer coating. Without effective cooling, this cover is going to melt and cause disaster effects. The combustor was a three-dimensional container. The width, height and length of this container was 111.8cm, 99.1cm and 156.9cm respectively. The container converged from X/L=0.51 and contraction angle was 15.8 degrees. Inlet and outlet cross-sectional area of the combustor simulator was 1.11m^2 and 0.62m^2. The test section contained two symmetric surfaces on the top and bottom of the combustor but the fluid only flowed through bottom passage. The lengths of the panels were 39cm, 41cm, 37 and 43 centimeters respectively. In addition, the first two panels were flat and have constant sectional area. However, the last two panels were inclined at the contraction angle and yield the exit sectional area of the combustor simulator. The panels were 1.27cm thick, and due to the low thermal conductivity (k=0.037 W/mk), adiabatic surface temperature measurements were possible. Dilution flow injection is beneficial to decline the temperature of the hot exit gases of the combustor simulator and prevent the detrimental effects of the critical components. Two different dilution rows were considered within the second and third panel of cooling panels. The dilution flow injected into the mainstream flow vertically, while, the dilution hole in the third panel was angled at 15.8° from the vertical axis. The first row of dilution jets included three holes and it was placed at 0.67m downstream of the combustor simulator inlet. These holes were 8.5cm in diameter. The second row contained two dilution holes and was located at 0.23m downstream of the first row of dilution holes center. These holes diameter was 1.4 times more than the first one at 12.1cm. The centerline of the second row was staggered with respect to those of the first row. In the present research, the combustor simulator contained four arrangements of cooling holes. For the verification of findings, the first arrangement (baseline or case 1) was designed similar to the Vakil and Thole [7] combustor simulator. As seen in Figure 1, The length of these cooling holes was 2.5cm and they drilled at an angle of 30° from the horizontal surface.

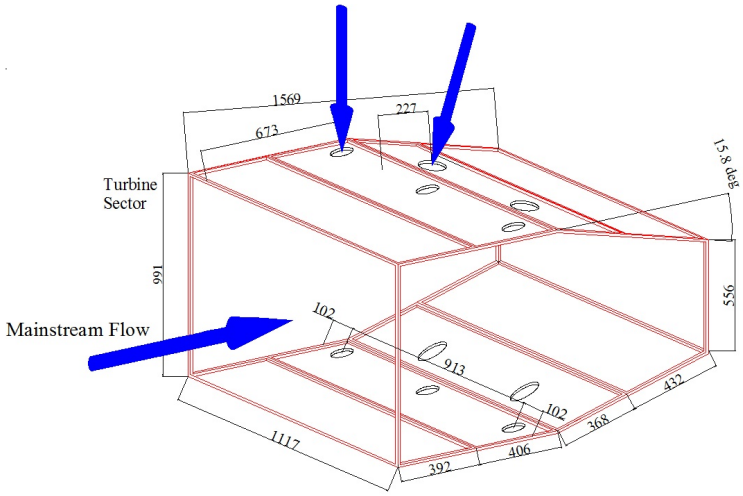

Fig. 1. Schematic view of the combustor simulator

The film-cooling holes were 0.76cm in diameter. Except the baseline case which introduced, to investigate the effects of cooling holes trenching, trenched spherical holes were considered. These holes have an elliptical cross section at the entrance of the cooling holes and starts to expand at a certain angle in a part of the hole path line and at the end of the cooling hole reaches to a new cross section shape (Figure 2).

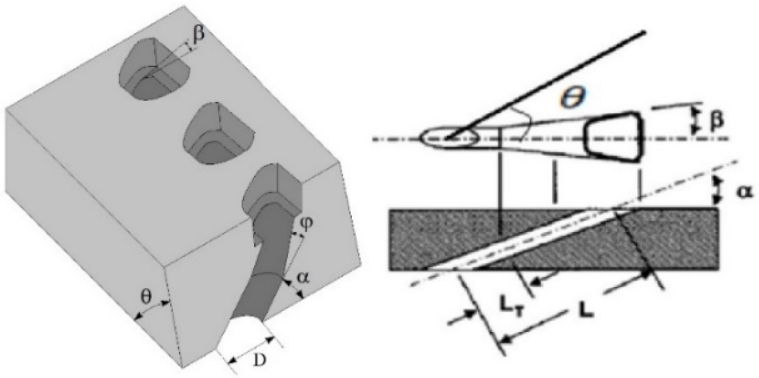

Fig. 2. (a) Schematic view of the combustor simulator (b) film cooling holes arrangement

The distance between the hole surface and the combustion chamber panel and the filler diameter on the spherical hole contact surface and the panel surface H=0.3, R=D/2=0.1, H=0.3, R=D/2=0.2 and H=0.3, R=D/2=0.3 cm. Other geometric parameters of cooling holes are shown in Table 1.

Table 1
Geometric parameters of cooling holes

parameter	quantity
β	0.6α
θ	α
L (cm)	2.5
L_f/L	0.4
H	0.8D

The Cartesian coordinate system (x, y and z) was selected. All coordinates were non-dimensionalized by the combustor simulator height (H_{in}), length (L) and width (W) respectively. The temperature of coolant and dilution jets was equal to 295.5 K. The temperature of mainstream was 332K. Figure 3 shows the observation planes which are used to measure the film-cooling effectiveness distribution for baseline case and three different configurations of row trenched cooling holes. The observation planes of P0, P1, P2, and P3 and S0 were placed in pitch wise and streamwise direction respectively. Plane P0 was located at x=35.1 cm. The distribution of film cooling momentum was computed along this panel. This plane lengthened within half of the combustor in the spanwise direction. The observation plane height extended from z=0cm to z=10cm. Plane P1 was located at the trailing edge of the first row of dilution jet. The importance of this plane was to identify the stream-wise behavior of the dilution jets first row. About 8×10^6 tetrahedral meshes were selected

(Figure 4). This quantity of nodes allowed appropriate convergence for corrected meshing; the thermal and flow characters would have the similar variation as the higher refinement mesh.

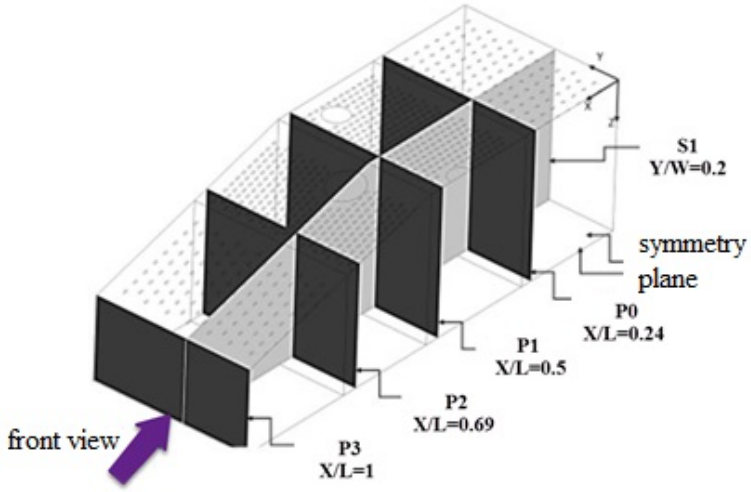

Fig. 3. Schematic view of the observation planes

2.2 Equations and Modelling

The numerical method considered a transient, incompressible turbulent flow by means of the *k–ε* turbulent model of the Navier–Stokes equations expressed as follows [15-21]:

Continuity equation

$$\frac{\partial}{\partial t}\left(\rho u_i\right)+\frac{\partial}{\partial x_j}=\left(\rho u_i u_j\right)=-\frac{\partial \mathrm{P}}{\partial x_i}+\frac{\partial \tau_{ij}}{\partial x_i}+\rho g_i+\vec{F}_1 \tag{1}$$

Momentum equation

$$\frac{\partial \rho}{\partial t}+\frac{\partial \rho}{\partial x}\frac{dx}{dt}+\frac{\partial \rho}{\partial y}\frac{dy}{dt}+\frac{\partial \rho}{\partial z}\frac{dz}{dt}=-\rho\left(\nabla . V\right) \tag{2}$$

Energy equation

$$\frac{\partial}{\partial t}\left(\rho E\right)+\frac{\partial}{\partial x_i}=\left(u_i\left(\rho E+P\right)\right)=\frac{\partial}{\partial x_i}\left(K_{eff}\frac{\partial T}{\partial x_i}-\sum\nolimits_j h_j J_j+u_i\left(\tau_{ij}\right)_{erf}\right)+S_h \tag{3}$$

and k–ε equation

$$\frac{\partial}{\partial t}\left(\rho k\right)+\frac{\partial}{\partial x_i}\left(\rho k u_i\right)=\frac{\partial}{\partial x_i}\left(\mu+\frac{\mu_t}{\sigma k}\frac{\partial k}{\partial x_j}\right)+P_k-\rho\varepsilon \tag{4}$$

$$\frac{\partial}{\partial t}\left(\rho \varepsilon\right)+\frac{\partial}{\partial x_i}\left(\rho \varepsilon u_i\right)=\frac{\partial}{\partial x_j}\left(\left(\mu+\frac{\mu_t}{\sigma\varepsilon}\right)\frac{\partial \varepsilon}{\partial x_j}\right)+C_{1\varepsilon}\frac{\varepsilon}{k}P_k-C_{2\varepsilon}^{*}\rho\frac{\varepsilon^2}{k} \tag{5}$$

To investigate the convergence limit, the control volume mass residue has been estimated and the maximum value has been used. For this research, the criterion of convergence has chosen 10^{-4}. The following equation is to determine the effectiveness of film-cooling.

$$\eta=\frac{T-T_\infty}{T_c-T_\infty} \tag{6}$$

Here T, T_∞ and T_c is the local temperature, the temperature mainstream and coolant respectively. Table 2 provides a list of parameters used in the governing equations for solving the problem.

Table 2
The list of parameters used in the equations

parameter	symbol	Measurement unit
density	ρ	Kg/m^3
velocity in x direction	u	m/s
pressure	P	kg/ms^2
gravity acceleration	g	m/s^2
viscosity stress	τ	Kg/ms^2
heat conduction coefficient	k	$Kgm/t^{-2}K$
specific energy	E	J/Kg
specific enthalpy	h	kJ/Kg
local temperature	T	K
mainstream temperature	T_∞	K
coolant temperature	T_c	K
film cooling effectiveness	η	-

2.3 The Model Numerical Solution

According to the considered blowing ratio at the inlet of control volume, the boundary condition of inlet mass flow was considered at the inlet. to limit the interaction region between fluid and combustor wall, slip-less boundary condition and wall boundary condition were considered. In addition, two different boundary conditions of uniform flow and pressure outlet was selected at the inlet and outlet of combustor respectively. Totally, according to the symmetries of the Pratt and Whitney gas turbine engine combustor, symmetry boundary condition was used. Gambit package was selected to mesh the combustor simulator and the model was analyzed by Fluent 6.2.26 software. About 8×106 tetrahedral meshes were selected (Figure 4).

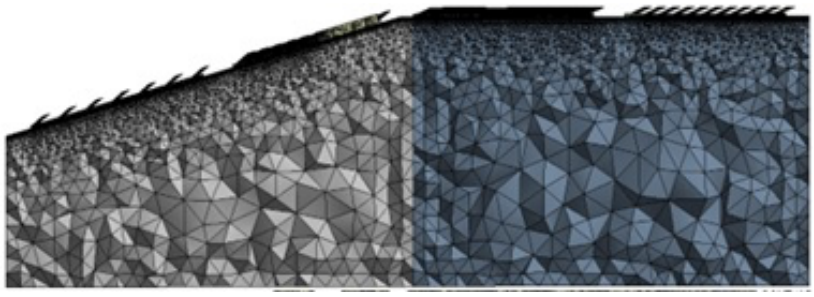

Fig. 4. Schematic view of the observation planes

In the case of the investigated meshes of the model, the combustor simulator domain has an increased mesh resolution due to the rectangular combustor being exposed to the complex flow effects. The mesh is refined in the grids from 1×10^6 to 8×10^6 where 7×10^6 and 8×10^6 represent coarse, medium, and fine mesh generated for the standard k-ε turbulence model. The average temperature increased from 314 to 321 as shown in Figure 5. The near-wall flow fields require special treatment. In RANS turbulent model, there are two main approaches for the determination of the shear-stress at a wall: Wall Function approach, which determine the shear-stress at the wall from semi-empirical equations, and Near Wall Model Approach. The y+ is the dimensionless quantity for the distance from

the wall up to the center of the first grid cell. Accurate presentation of the flow in the near-wall region determines successful prediction of wall-bounded turbulent flows. Values of y^+ In the Wall Function Approach method (y^+>30) are most desirable for wall functions (Figure 6).

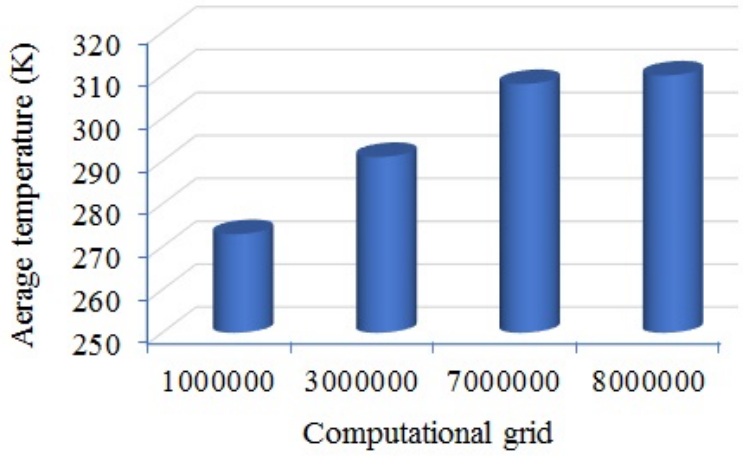

Fig. 5. The average temperature of all the investigated meshes in mesh independency study

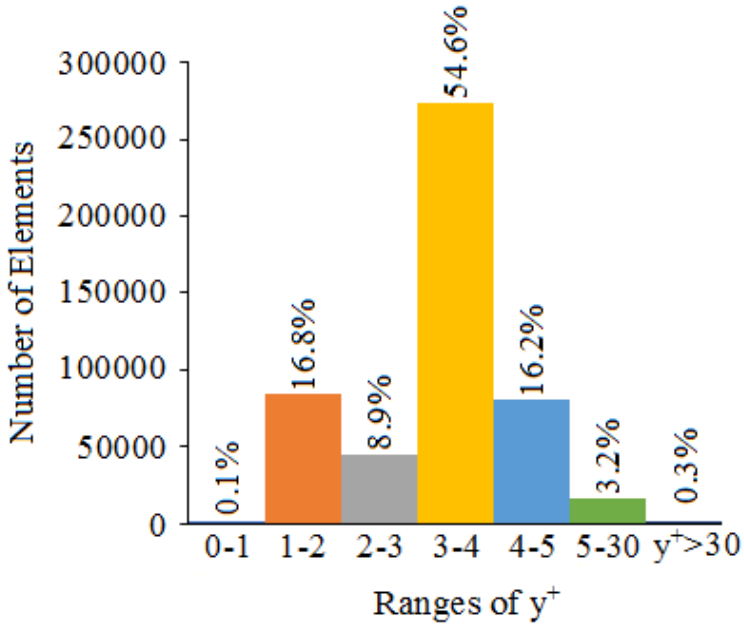

Fig. 6. Corresponding wall y^+

3. Results

The findings of the current research were compared with the experimental collected results which was done by Vakil and Thole [7]. The effectiveness of film-cooling was compared in plane P1 at y/w=0.25 (Figure 7). The deviations between the results of current research and benchmarks were computed by the following equation. The deviation was equal to 5% compared to Vakil and Thole measurements [7] for plane P1.

$$\%Diff = \frac{\sum_{i=1}^{n} \frac{x_i - x_{i,benchmark}}{x_{i,benchmark}}}{n} \times 100 \quad (7)$$

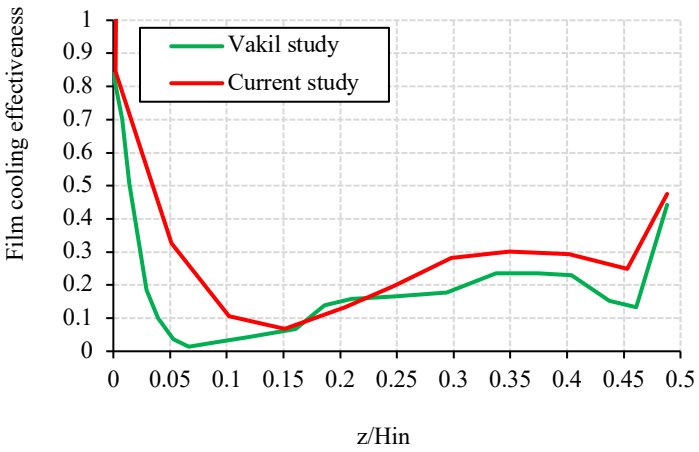

Fig. 7. The film cooling effectiveness comparison of plane P1 along y/W=0.25

Figures 8 and 9 show the averaged film cooling effectiveness at different trench radiuses from 0.1 to 0.3 and constant height on observation plane P1 and P2. As can be seen, in the middle of the combustor simulator and at a distance of 0.01cm<z<0.06cm, with H=0.3 and R=0.2 cm, a spherical hole has the highest film cooling effectiveness. At the end of the combustor simulator, the film cooling effectiveness is similar for all three types of trench spherical holes. This indicates an increase in the penetration of the dilution jets into the spherical hole with H=0.3 and R=0.2 cm, which improves the film cooling effectiveness in the combustor simulator. According to the results obtained from numerical analyzes, the application of spherical trenched holes with different heights will increase the film cooling effectiveness and reduce the temperature of the combustor simulator. On the other hand, along the combustor, the spherical hole with H=0.3 and R=0.2 cm has the highest film cooling effectiveness.

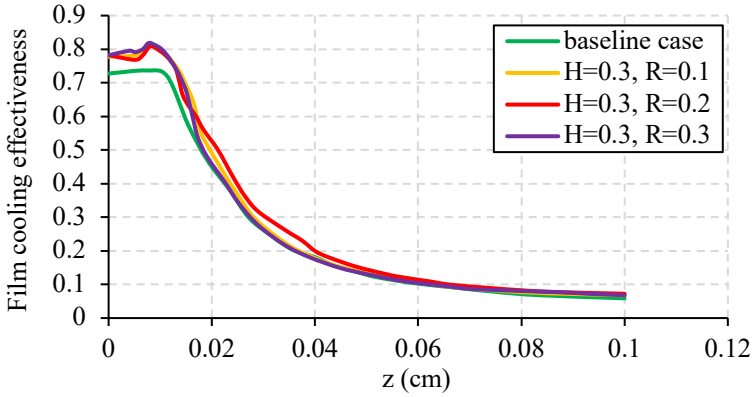

Fig. 8. Averaged film cooling effectiveness distribution for plane P1

The effectiveness of film cooling in observation plane P2 at blowing ratio of 3.18 is shown in Figure 10. The most important difference between these schemes is the coolant injection into the

main flow. Exactly downstream the second row of dilution jets, more effective coolant layer (10cm<y<50cm) was formed by the trenched holes with H=0.3 and R=0.2 cm on the critical surfaces downstream the combustor simulator. The significant protective layer (0.9<η<1.0) was seen for the row trenched holes with H=0.3 and R=0.2 cm. Also, the results show that at height of R=0.2 and R=0.3cm, the cooling absorption of the layer adjacent to the wall is weaker. The reason for this is to reduce the penetration of the cooling current due to the reduction of the flow turbulence. This reduces heat transfer and weakens the film cooling on the combustion chamber panels. For the trenched holes with H=0.3 and R=0.2 cm, the maximum height of the layer was 20 cm, equal to 20% of the combustor inlet height. This gave the highest cooling layer among all the cases.

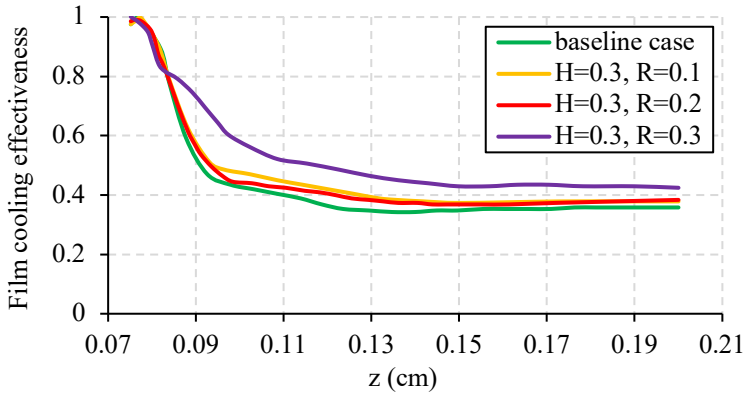

Fig. 9. Averaged film cooling effectiveness distribution for plane P1

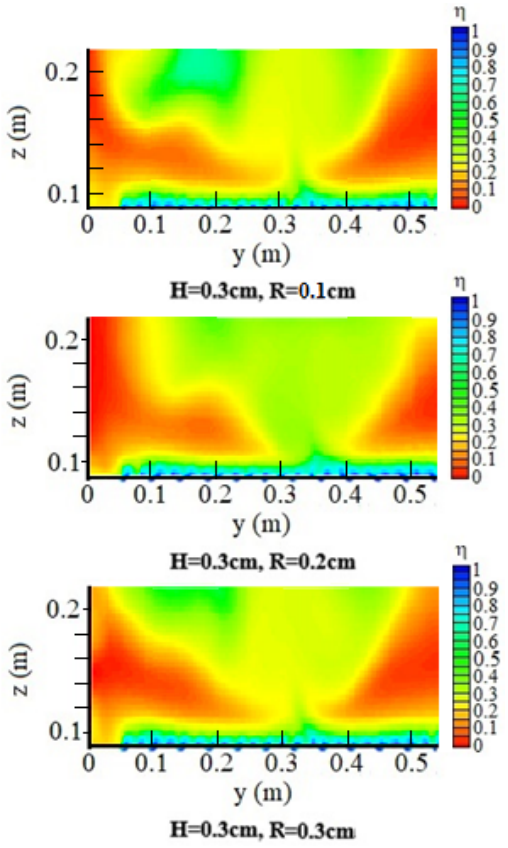

Fig. 10. Film cooling effectiveness in plane P2

In Figure 11, the film cooling effectiveness distribution on the observation plane of S1 at different heights from R=0.1cm to R=0.3cm and constant radius R=0.2 cm is shown. As can be seen, the spherical hole with H=0.3cm and R=0.2cm has the lowest film cooling effectiveness throughout the combustor simulator. As can be seen, the temperature contours immediately behind the jet show a thinner layer of film cooling when the flow is entrained into the jet. Much of the film-coolant was entrained and carried away by the dilution jet right at the trailing edge, thus leaving behind a thinner film of coolant. This entrainment, or recirculating region behind the dilution jet, could also be seen within observation plane of S1. In the first half of the combustion chamber, at 0m<z<0.3m, the cooling efficiency of the cavity with R=0.3cm is higher and has a higher cooling effectiveness. But in the second half of the combustion chamber, at 0.3m<z<0.5m, this procedure is reversed and the cooling effectiveness of the hole with R=0.2cm is higher and has a higher cooling effectiveness.

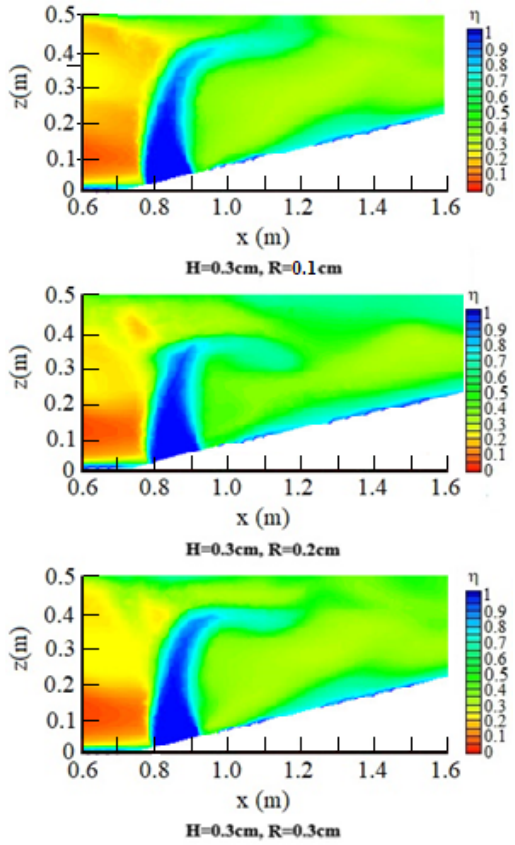

Fig. 11. Film cooling effectiveness of plane S1

4. Conclusions

In this research a computational study was conducted in order to have a better understanding of the film cooling effectiveness and the effects of cylindrical and spherical trenched cooling holes with surface H=0.3,R=D/2=0.1, H=0.3, R=D/2=0.2 and H=0.3, R=D/2=0.3 from the combustor exit of a gas turbine engine at BR=3.18. An optimize design cooling holes will help to maximize the effectiveness of cooling along the combustor end wall surface and prevent premature wear in this area. A three-dimensional representation of a gas turbine engine was simulated in order to analyse the effects of cylindrical spherical trenched cooling holes on film cooling performance. The combustor simulator combined the effects of two rows of stream-wise staggered and span-wise aligned dilution jets. The commercial FLUENT software and RNG k-ε turbulence model were

employed to run the computations on the thermal fields within a combustor simulator. Compared to baseline method, in the trenched case, the coolant stayed closer to the end wall surface and did not allow main entrainment. Comparisons between the data computationally predicted and those collected by Vakil and Thole [7] indicate the existence of similarities and differences. The results show that it is more desirable to use this hole geometry so that the film cooling effectiveness increase in about 48 percent on observation planes of P1 and P2.

References

[1] Elmahi, Abdelbaki, Touhami Baki, and Mohamed Tebbal. "New analysis of experimental data of the hydrodynamic liquid film around jet zone on horizontal plate." *Archive of Mechanical Engineering* 68, no. 4 (2021).

[2] Harrington, Mark K., Marcus A. McWaters, David G. Bogard, Christopher A. Lemmon, and Karen A. Thole. "Full-coverage film cooling with short normal injection holes." *J. Turbomach.*123, no. 4 (2001): 798-805. https://doi.org/10.1115/1.1400111

[3] Koc, Ibrahim, Yaşar İslamoğlu, and Ünal Akdağ. "Investigation of film cooling effectiveness and heat transfer coefficient for rectangular holes with two rows." *Aircraft Engineering and Aerospace Technology* (2009). https://doi.org/10.1108/00022660910941794

[4] Azzi, Abbes, and B. Jubran. "Numerical modeling of film cooling from short length stream-wise injection holes." *Heat and mass transfer* 39, no. 4 (2003): 345-353. https://doi.org/10.1007/s00231-002-0320-0

[5] Bernsdorf, Stefan, Martin G. Rose, and Reza S. Abhari. "Modeling of film cooling—Part I: experimental study of flow structure." (2006): 141-149. https://doi.org/10.1115/1.2098768

[6] Tarchi, Lorenzo, Bruno Facchini, Francesco Maiuolo, and Daniele Coutandin. "Experimental investigation on the effects of a large recirculating area on the performance of an effusion cooled combustor liner." *Journal of Engineering for Gas Turbines and Power* 134, no. 4 (2012). https://doi.org/10.1115/1.4004729

[7] Vakil, Sachin S., and Karen Ann Thole. "Flow and thermal field measurements in a combustor simulator relevant to a gas turbine aeroengine." *J. Eng. Gas Turbines Power* 127, no. 2 (2005): 257-267. https://doi.org/10.1115/1.1806455

[8] Kianpour, Ehsan, Nor Azwadi Che Sidik, and Iman Golshokouh. "Measurement of film effectiveness for cylindrical and row trenched cooling holes at different blowing ratios." *Numerical Heat Transfer, Part A: Applications* 66, no. 10 (2014): 1154-1171. https://doi.org/10.1080/10407782.2014.901042

[9] Azwadi, Nor, and Ehsan Kianpour. "The Effect of Blowing Ratio on Film Cooling Effectiveness Using Cylindrical and Row Trenched Cooling Holes with Alignment Angle of 90 Degrees." *Mathematical Problems in Engineering* 2014 (2014). https://doi.org/10.1155/2014/470576

[10] Schuchkin, V., M. Osipov, Wei Shyy, and S. Thakur. "Mixing and film cooling in supersonic duct flows." *International journal of heat and mass transfer* 45, no. 22 (2002): 4451-4461. https://doi.org/10.1016/S0017-9310(02)00151-5

[11] Li, Yifei, Yang Zhang, Xinrong Su, and Xin Yuan. "Experimental and numerical investigations of shaped hole film cooling with the influence of endwall cross flow." *International Journal of Heat and Mass Transfer* 120 (2018): 42-55. https://doi.org/10.1016/j.ijheatmasstransfer.2017.11.150

[12] Fraas, Marc, Tobias Glasenapp, Achmed Schulz, and Hans-Jörg Bauer. "Optimized inlet geometry of a laidback fan-shaped film cooling hole–experimental study of film cooling performance." *International Journal of Heat and Mass Transfer*128 (2019): 980-990. https://doi.org/10.1016/j.ijheatmasstransfer.2018.09.035

[13] Chen, Da-wei, Hui-ren Zhu, Cun-liang Liu, Hua-tai Li, Bing-ran Li, and Dao-en Zhou. "Combined effects of unsteady wake and free-stream turbulence on turbine blade film cooling with laid-back fan-shaped holes using PSP technique." *International Journal of Heat and Mass Transfer* 133 (2019): 382-392. https://doi.org/10.1016/j.ijheatmasstransfer.2018.12.102

[14] Kim, Sun-Min, Ki-Don Lee, and Kwang-Yong Kim. "A comparative analysis of various shaped film-cooling holes." *Heat and Mass Transfer* 48, no. 11 (2012): 1929-1939. https://doi.org/10.1007/s00231-012-1043-5

[15] Niknahad, Ali. "Numerical study and comparison of turbulent parameters of simple, triangular, and circular vortex generators equipped airfoil model." *Journal of Advanced Research in Numerical Heat Transfer* 8, no. 1 (2022): 1-18.

[16] El-Okda, Yasser M., and Ghassan Nasif. "Conjugate Effect on the Heat Transfer Coefficient." *Journal of Advanced Research in Numerical Heat Transfer* 5, no. 1 (2021): 1-8.

[17] Widiawaty, Candra Damis, Ahmad Indra Siswantara, Gun Gun R. Gunadi, Mohamad Arif Andira, Muhammad Arif Budiyanto, M. Hilman Gumelar Syafei, and Dendy Adanta. "Optimization of inverse-Prandtl of Dissipation

in standard k-ε Turbulence Model for Predicting Flow Field of Crossflow Turbine." *CFD Letters* 14, no. 1 (2022): 112-127. https://doi.org/10.37934/cfdl.14.1.112127

[18] Wang, Lingquan, Ge Nie, Liwei Xiao, Guanyun Zhao, Yueyong Chen, and Chunhua Wei. "Applications of Computational Fluid Dynamics in the E-Cigarettes Industry." *Journal of Advanced Research in Fluid Mechanics and Thermal Sciences* 96, no. 1 (2022): 70-81. https://doi.org/10.37934/arfmts.96.1.7081

[19] Sathishkumar, Shriram, Bommisetty Sambasiva Rao, Sidharth Pradeep, Solai Sairam RM, Balaji Kalaiarasu, and Prabhu Selvaraj. "Modelling and Validating the Spray Characteristics of a Co-axial Twin-Fluid Atomizer Using OpenFOAM." *Journal of Advanced Research in Fluid Mechanics and Thermal Sciences* 91, no. 1 (2022): 35-45. https://doi.org/10.37934/arfmts.91.1.3545

[20] Tey, Wah Yen, Yutaka Asako, Nor Azwadi Che Sidik, and Rui Zher Goh. "Governing equations in computational fluid dynamics: Derivations and a recent review." *Progress in Energy and Environment* 1 (2017): 1-19.

[21] Al Mahmud, Suaib, Ahmad Faris Ismail, Jamirul Habib Bappy, and Wazed Ibne Noor. "Mixture Model for a Parametric Study on Turbulent Convective Heat Transfer of Water-Al2O3 Nanofluid." *CFD Letters* 14, no. 2 (2022): 42-58. https://doi.org/10.37934/cfdl.14.2.4258